JACS
JOURNAL OF THE AMERICAN CHEMICAL SOCIETY

COMMUNICATION

pubs.acs.org/JACS

Synthesis of PbSeTe Single Ternary Alloy and Core/Shell Heterostructured Nanocubes

Zewei Quan,[†] Zhiping Luo,[‡] Welley Siu Loc,[†] Jun Zhang,[†] Yuxuan Wang,[§] Kaikun Yang,[∥] Nathan Porter,[†] Jun Lin,[⊥] Howard Wang,[∥] and Jiye Fang*[,†,§]

[†]Department of Chemistry, [§]Materials Science and Engineering Program, and [∥]Department of Mechanical Engineering, State University of New York at Binghamton, Binghamton, New York 13902, United States

[‡]Microscopy and Imaging Center and Materials Science and Engineering Program, Texas A&M University, College Station, Texas 77843, United States

[⊥]State Key Laboratory of Rare Earth Resource Utilization, Changchun Institute of Applied Chemistry, Chinese Academy of Sciences, Changchun 130022, P.R. China

Supporting Information

ABSTRACT: We report a robust method for synthesis of monodisperse PbSeTe single ternary alloy and core/shell heterostructured nanocubes, respectively. The key synthetic strategy to produce such different classes of nanocubes is to precisely control the time of reaction and successive growth. The crystallinity, shape/size distributions, structural characteristics, and compositions of as-prepared nanocubes, both ternary alloy and core/shell, were carefully studied. A plausible growth mechanism for developing each type of lead chalcogenide nanocubes is proposed. These delicately designed PbSeTe nanoscale architectures offer tunable compositions in PbSeTe ternary alloy and nano-interfaces in core/shell nanocubes, which are the critical factors in controlling thermal conductivity for applications in thermoelectrics.

Many recent advances in enhancing the thermoelectric figure of merit ($ZT = S^2\sigma T/\kappa$) can be attributed to the nanocomponents presented. For example, quantum-confinement effects in the nanomaterials could enhance the Seebeck coefficient (S) as well as the electrical conductivity (σ), while nanoscaled internal interfaces may reduce the thermal conductivity (κ) in their respective scattering lengths.[1] Lead chalcogenides, especially PbSe and PbTe, are ideal materials for thermoelectric applications due to their large Bohr exciton radii (strong quantum-confinement effects) and low thermal conductivity.[2,3] Numerous research reports have indicated that the thermal conductivity could be further lowered by either introducing a third component into the building blocks to form a ternary alloy (e.g., PbSeTe) or even a quaternary alloy, or fine-tuning the "nano-interfaces" to form heterostructures (e.g., core/shell) due to their boundary-enhanced phonon scattering effects.[1,4−6] One of the innovative approaches in colloidal chemistry that enables the fabrication of lead chalcogenides nanocrystals with size and shape control is organic solution-based high-temperature synthesis.[7−10] The resultant nano-building blocks, with controllable spatial distribution and modulated compositions, were demonstrated as superior thermoelectric materials in solid-state cooling and electrical power generation devices.[1,4,5,11] In comparison with preparation of other types of complex chalcogenides, such as PbSSe,[12,13] CdSe-ZnS,[14] and PbSe-PbS,[12,15] fewer publications on the synthesis of high-quality ternary alloy or core/shell heterostructured PbSe and PbTe are available,[16] probably due to the large difference in the reaction activity between Se and Te.

In our previous studies, we successfully prepared various lead chalcogenide nanostructures (e.g., PbSe nanocubes, PbTe nanocubes, PbSe:Mn nanoarrays).[17−20] These achievements encouraged us to explore the possibility of extending this synthetic strategy to produce PbSeTe ternary alloy and core/shell nanostructures, which possess unusual physical characteristics for sustainable energy resource exploration. Considering that the reactivity of Te-TOP is higher than that of Se-TOP (Te has a weaker electron-accepting capability versus Se,[21] and therefore Te-TOP is relatively unstable), it is possible to harvest either PbSeTe ternary alloy or core/shell heterostructured nanocubes by simply adjusting the relative formation times of PbSe and PbTe when PbTe is designed to diffuse into or grow on existing PbSe nuclei. Herein, we present a successive growth approach utilizing the activity difference between Se and Te precursors to obtain two unique nanostructures composed of PbSe and PbTe. Other experimental parameters, such as the influence of precursor ratio on the composition of PbSeTe ternary alloy nanocubes, are also investigated.

Nanocrystal synthesis was conducted under an Ar atmosphere using a standard air-free Schlenk line technique. Based on our previous strategy with improved processing control,[17−20] a sequential injection method was developed to prepare PbSeTe ternary alloy and core/shell nanocubes in this work. (1) For PbSeTe ternary alloy nanocubes, in a typical experiment, 3 mmol of Pb-oleate was prepared first (experimental details are given in the Supporting Information (SI)). After that, 2.8 mL of Se-TOP (1 M) and 14.0 mL of diphenyl ether were heated to 200 °C for 10 min, and the as-prepared Pb-oleate solution was rapidly injected into this system to form PbSe nuclei. At the 11th sec after such an injection, a black transparent solution was observed, and 0.2 mL of Te-TOP solution (1 M) was then introduced immediately. Reaction in the system was ceased 6 min after the Te-TOP injection by promptly replacing the heating source with

Received: August 16, 2011
Published: October 06, 2011

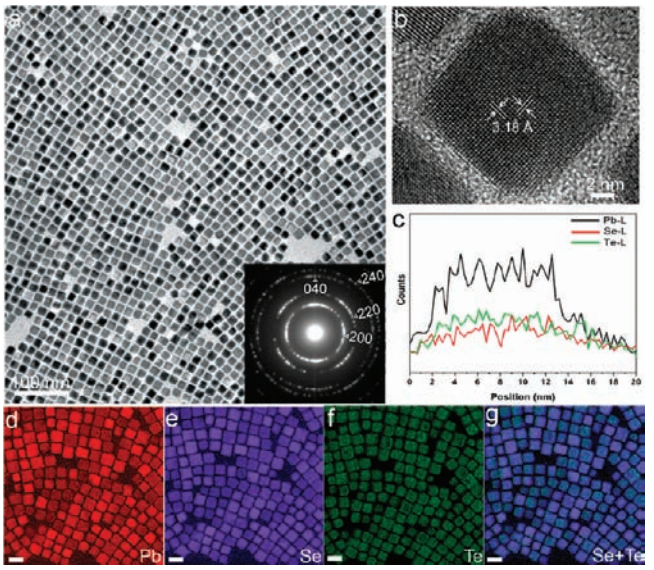

Figure 1. Images of PbSeTe single ternary alloy nanocubes. (a) TEM image; inset is an SAED pattern. (b) HR-TEM image and (c) HAADF-STEM EDS line scan profile of an individual nanocube. (d−g) Elemental maps of Pb (red), Se (purple), Te (green), and Se+Te overlap, respectively; scale bars represent 20 nm.

a cold water bath. These nanocubes, denoted as $Pb_3Se_{2.8}Te_{0.2}$, were eventually stored in hexane, forming a colloidal solution. By tuning the ratio between Se-TOP and Te-TOP within a total amount of 3 mmol while the other conditions were kept the same, various PbSeTe ternary alloy nanocubes, denoted as $Pb_3Se_{1.5}Te_{1.5}$, $Pb_3Se_{2.5}Te_{0.5}$, $Pb_3Se_{2.6}Te_{0.4}$, $Pb_3Se_{2.7}Te_{0.3}$, $Pb_3Se_{2.8}Te_{0.2}$, and $Pb_3Se_{2.9}Te_{0.1}$, were prepared using this method. (2) For PbSeTe core/shell nanocubes, the procedure for their preparation is almost the same as above, except that 0.2 mL of Te-TOP (1 M) was injected into the system 4 or 5 min after the formation of PbSe nuclei (rather than at the 11th sec).

Figure 1a shows a typical transmission electron microscopy (TEM) image of PbSeTe ternary alloy nanocubes, demonstrating a perfect cubic morphology and relatively uniform size distribution with an average side length of 11.0 ± 0.5 nm (based on 50 nanocubes). It also exhibits a "square-ordered" pattern: each nanocube is surrounded by four other neighboring nanocubes, showing a specific pattern in the nanocube monolayer. Due to their uniformity in both size and shape, PbSeTe single ternary alloy nanocubes can also be assembled into multilayered supercrystals with characteristic dimensions on the order of micrometers, as illustrated in Figure S1. Scanning electron microscopy (SEM) observation suggests that the surface of this supercrystal possesses many common features as in the case of atoms on a crystal surface, such as terraces, ledges, and kinks. Looking along the direction perpendicular to the wafer surface, the array of all the nanocubes appears flat with respect to the substrate surface, which was classified as a "simple cubic supercrystal".[20,22] A selected-area electron diffraction (SAED) pattern is also provided, which shows the nanocubes are all [001] oriented and well aligned to exhibit textured features. Careful inspection, with astigmatism corrected and well in focus, reveals a single lattice; i.e., all the reflection spots are in the rings from a single lattice. High-resolution TEM (HR-TEM) of a PbSeTe single ternary alloy nanocube (Figure 1b) shows clear lattice fringes, with an interfringe distance of ~3.18 Å over the entire

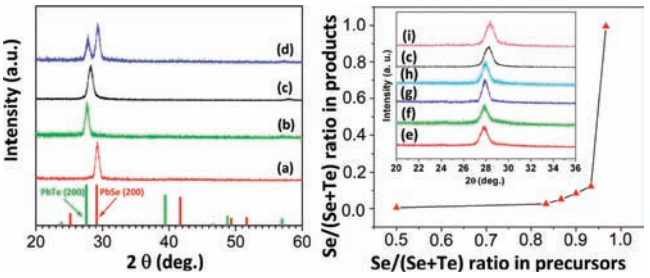

Figure 2. (Left) XRD patterns of (a) PbSe nanocubes, (b) PbTe nanocubes, (c) $Pb_3Se_{2.8}Te_{0.2}$ single ternary alloy nanocubes, and (d) mixture of PbSe and PbTe nanocubes. Standard patterns from ICDD PDF cards (06-0354 for PbSe in red and 38-1435 for PbTe in green) are shown at the bottom. (Right) XRD patterns of (e) $Pb_3Se_{1.5}Te_{1.5}$ nanocubes, (f) $Pb_3Se_{2.5}Te_{0.5}$ nanocubes, (g) $Pb_3Se_{2.6}Te_{0.4}$ nanocubes, (h) $Pb_3Se_{2.7}Te_{0.3}$ nanocubes, and (i) $Pb_3Se_{2.9}Te_{0.1}$ nanocubes together with (c) $Pb_3Se_{2.8}Te_{0.2}$ nanocubes as reference, as well as the corresponding ICP-OES plot of the molar ratio of Se/(Se+Te) in final products as a function of that in the precursors. All of the samples for XRD characterizations were assembled on a polished 25 mm Si (100) wafer.

nanocube surface, which falls between the {200} lattice spacings of PbSe (3.06 Å) and PbTe (3.23 Å). This analysis suggests that the as-prepared PbSeTe is a uniform alloy without a heterogeneous structure. High-angle annular dark-field imaging in the scanning TEM (HAADF-STEM) mode energy dispersive X-ray spectroscopy (EDS) line scanning analysis (Figure 1c) also reveals the compositional variation over a single nanocube. The EDS intensity profiles of Pb, Se, and Te were plotted as a function of the distance crossing the nanocube, showing uniform distributions of Pb, Se, and Te through the scanned area. This further verifies a ternary alloy structure in the as-formed PbSeTe. Images in Figure 1d−g show the electron energy loss spectroscopic (EELS) elemental mapping results for Pb (red), Se (purple), Te (green), and the Se+Te overlap, indicating an even distribution for both Se and Te elements. This is an additional piece of evidence to confirm the ternary alloy structure.

To further examine the microstructures of these nanocubes, a typical X-ray diffraction (XRD) pattern of $Pb_3Se_{2.8}Te_{0.2}$ nanocubes is presented in Figure 2c (left panel). For comparison with this pattern, XRD traces of PbSe nanocubes[23] (Figure 2a), PbTe nanocubes[23] (Figure 2b), and their mixture (Figure 2d), standard patterns from ICDD PDF cards (Figure 2, bottom of the left panel), as well as traces recorded from two classes of typical nanocubes *without* assembly (Figure S2, all the detectable XRD peaks were shown) are also given. In each of these assembled patterns, only one strong peak, indexed to the (200) plane, is observed, indicating that these nanocubes align perfectly on the surface-polished Si wafer with {100} texture.[20,24,25] This results in a significant enhancement of (200) peaks and absence of other peaks. This macroscale observation further supports that the nanocubes terminated with {100} facets are dominant in the final products. The position of the (200) peak in the pattern of $Pb_3Se_{2.8}Te_{0.2}$ nanocubes (Figure 2c) implies formation of a PbSeTe ternary alloy rather than mixed phases of PbSe and PbTe (Figure 2d), as the single peak is located between those of pure PbSe (Figure 2a) and PbTe nanocubes (Figure 2b) and no diffraction signal of PbSe and/or PbTe was detected in Figure 2c.

PbSeTe single ternary alloy nanocubes with adjustable compositions were also prepared by precisely tuning the ratio between the chalcogenide precursors, Se-TOP and Te-TOP. XRD patterns of the samples including (e) $Pb_3Se_{1.5}Te_{1.5}$, (f) $Pb_3Se_{2.5}Te_{0.5}$, (g)

$Pb_3Se_{2.6}Te_{0.4}$, (h) $Pb_3Se_{2.7}Te_{0.3}$, (c) $Pb_3Se_{2.8}Te_{0.2}$, and (i) $Pb_3Se_{2.9}Te_{0.1}$ nanocubes, together with their corresponding inductively coupled plasma optical emission spectrometric (ICP-OES) results, are shown in the right panel of Figure 2, revealing clearly that the XRD patterns shift to higher positions of 2θ with increasing Se/Te ratio in precursors. (For comparison purposes, only selected ranges of the XRD patterns are presented.)[24] This is in good agreement with Vegard's law. The actual molar percentage of Se (Se/(Se+Te)) in the final products was determined through ICP-OES analysis and is plotted as a function of the input values in their precursors (also refer to Table S1). This curve indicates a crucial window for the molar ratio of Se/(Se+Te) in the precursors, from 0.83 to 0.93, to harvest PbSeTe ternary alloy nanocubes. Beyond this input window, almost pure PbTe or PbSe nanocubes would be produced, and no linear relationship between the input and product can be found. For example, incorporation of 93 atom% Se in the precursors resulted in PbSeTe ternary alloy nanocubes with 12 atom% Se only, whereas the Se composition in the products rapidly increased when the amount of Se in the precursors was increased to ~95 atom% or higher. It should be noted that, due to the large difference in reactivity between Se and Te precursors, PbTe was the only product presented with no observable Se component when both Se and Te precursors (Se-TOP and Te-TOP) were simultaneously added into the reaction system without using the as-developed successive growth method, regardless of the molar ratio of Se/(Se+Te) precursors. This observation indicates that the as-developed sequential injection method is an essential strategy to "drag" the Se ions into PbTe lattices to form PbSeTe ternary alloy nanocubes.

It is believed that the size of PbSe nuclei should be pretty small at the time when Te-TOP is rapidly introduced into the reaction system. In that case, complete diffusion of Te into the PbSe lattice is possible to ensure formation of uniform PbSeTe ternary alloy nanocubes. The mechanism of this growth process is supported by XRD study on the *in situ* isolated intermediates. Figure S3 shows that the (200) peak downshifts gradually, indicating an increased Te composition in the samples as the reaction is proceeding. As discussed above, the initial formation of PbSe nuclei is the key to obtaining PbSeTe ternary alloy nanocubes; however, there is an upper limit for the size of PbSe nuclei. If the reaction time for PbSe growth is longer, PbSe nuclei will accordingly be larger, making the complete diffusion of Te atoms into PbSe nuclei more difficult. Further extension of the PbSe growth time to a certain value (4 min in this case) could result in growth of PbSe to a critical size that allows only partial penetration of Te atoms, introduced on a delayed time scale, into the PbSe lattice. Instead of diffusion into PbSe with such "hard cores", the "freshly" introduced Te precursors prefer to form "shells" with the presence of Se residuals, generating heterostructured PbSeTe core/shell nanocubes. Figure 3 summarizes both reaction mechanisms proposed above.

When Te-TOP was injected 4 min (or later) after PbSe growth, heterostructured nanocubes rather than PbSeTe ternary alloy nanocubes were produced. As illustrated in Figures 4a and S2, the XRD patterns of $Pb_3Se_{2.8}Te_{0.2}$ ternary alloy nanocubes (black) are different from those of core/shell nanocubes (red). In the core/shell patterns, the broad peak actually contains (200) peaks of possibly two phases, whereas such a peak in the ternary alloy sample can be indexed to PbSeTe ternary alloy nanocubes only. These results provide strong evidence for formation of heterostructures instead of a single phase. Figure 4b presents a TEM image of the PbSeTe core/shell nanocubes. Those with an

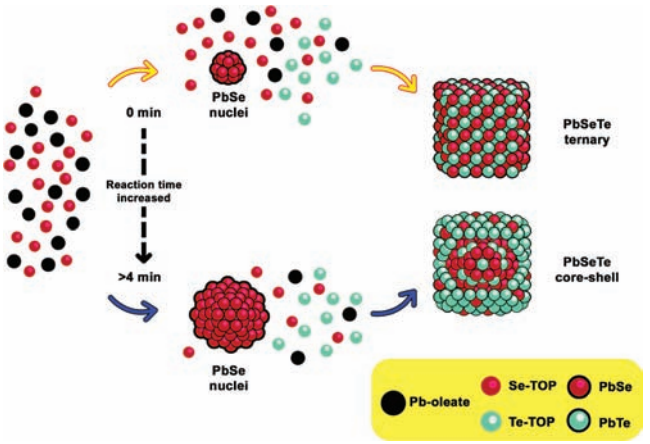

Figure 3. Schematic illustration depicting the formation of PbSeTe single ternary alloy and core/shell nanocubes.

average side length of ~11 nm possess a very narrow size distribution, with standard deviation <3% (based on 50 nanocubes). An SAED pattern is shown in the inset of Figure 4b, with special precaution exercised to avoid any astigmatism or unfocus. Apparent double rings can be observed, as indicated by double markers. The distance between the double rings is related to the scattering angle, or the radius of the ring. At higher scattering angles, the distance is larger. The radius of the first ring is too small to be evident in the pattern. The compositional architecture of these core/shell nanocubes was further supported by HAADF-STEM EDS line scan analysis across one nanocube. Figure 4c suggests that more Se is present in the center and more Te is distributed along the "edges", as shown in the circled area. Note that, due to the spurious signals in the EDS from the surrounding areas,[26] the line scan profiles do not correspond to the core/shell positions, as the scale is so small. A high-magnification image is shown in Figure 4d, and a corresponding weak-beam dark-field (WBDF) image of this area is presented in Figure 4e, depicting shell structures and indicating double lattices due to the strain field induced by the mismatch between the shell and core. A HRTEM image of the circled particle in Figure 4d is shown in Figure 4f, which reveals complex features formed by the interference of these two lattices. Furthermore, this result is confirmed by their EELS elemental mapping results (Figure 4g–j), in which Pb is seen uniformly distributed in the nanocubes and Te prefers to reside in only portions of the shells, whereas more Se appears in the cores. From the WBDF image and Te map, the shell thickness is estimated as 1.0 ± 0.2 nm based on 10 measurements with clear shells; therefore, the volume of the core is $9^3 = 729$ nm^3, and that of the shell is $11^3 - 9^3 = 602$ nm^3. The volume fraction of the core is 0.548, and that of the shell is 0.452. EDS analysis (Figure S4) of this core/shell sample reveals a composition of 47.7 atom% Pb, 18.8 atom% Se, and 33.5 atom % Te; thus, the Se/Te content ratio is $C_{Se}/C_{Te} = 0.561$. If the core (0.548 volume fraction) is purely $Pb_{0.5}Se_{0.5}$ and the shell (0.452 volume fraction) is purely $Pb_{0.5}Te_{0.5}$, the Se and Te contents would be $C_{Se} = 0.5 \times 0.548 = 0.274$ and $C_{Te} = 0.5 \times 0.452 = 0.226$. The measured composition showed lower Se content but higher Te, which indicates Te may partially occupy the core as well. Suppose the core composition is $Pb_{0.5}Se_xTe_{0.5-x}$, and that of the shell is $Pb_{0.5}Se_yTe_{0.5-y}$—according to the C_{Se}/C_{Te} ratio, it is found that x is in the range of 0–0.328, while $y = 0.398-1.212x$ to keep the C_{Se}/C_{Te} ratio, and $x \gg y$ as Se is

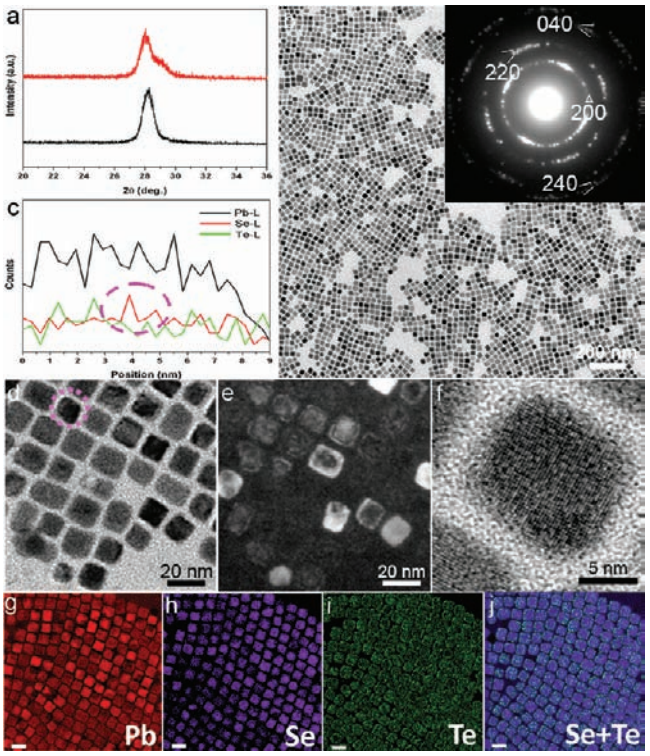

Figure 4. (a) XRD patterns of PbSeTe core/shell nanocubes (red) and $Pb_3Se_{2.8}Te_{0.2}$ single ternary alloy nanocubes (black); both samples were assembled on a polished 25 mm Si (100) wafer. (b,d) TEM images [inset of (b): SAED pattern] and (c) HAADF-STEM EDS line scan profile of PbSeTe core/shell nanocubes. (e) WBDF image. (f) HRTEM image of a single PbSeTe core/shell nanocube. (g–j) Elemental maps of Pb (red), Se (purple), Te (green), and their Se+Te overlap, respectively; scale bar, 20 nm.

observed in the core area (for details, refer to the SI). An example of the solution is given as the core $Pb_{0.5}Se_{0.3}Te_{0.2}$ and the shell $Pb_{0.5}Se_{0.034}Te_{0.466}$ in the SI. This suggests that significant Te is indeed involved in the core structure, whereas in the shell Se is very low or absent (meaning only PbTe is present). In both the core and the shell, Pb accounts for 0.5 of the composition, which is believed to stabilize the lead chalcogenide structure.

In summary, we have developed a robust synthesis route to prepare high-quality PbSeTe ternary alloy and core/shell nanocubes through fine control of the PbSe nucleation time. Shape control and modulation of element distribution in a nanocube could be achieved by diffusion or epitaxial growth of PbTe into or over the preformed PbSe nuclei for ternary alloy or core/shell syntheses, respectively. A plausible crystal growth mechanism of such a synthesis has also been proposed. Furthermore, preparation of relatively long-range ordered supercrystals using PbSeTe ternary alloy nanocubes was demonstrated, suggesting that these nanocubes could be promising building blocks in development of nanodevices with anisotropic structure.

■ ASSOCIATED CONTENT

Supporting Information. Chemicals and experimental procedure, characterization details, SEM images, ICP-OES results, XRD patterns of intermediates and products, EDS spectrum and results on PbSeTe core/shell nanocubes, and composition discussion. This material is available free of charge via the Internet at http://pubs.acs.org.

■ AUTHOR INFORMATION

Corresponding Author
jfang@binghamton.edu

■ ACKNOWLEDGMENT

This project is supported by NSF (DMR-0731382 and CMMI-0928865). J.L. acknowledges the National Basic Research Program of China (2007CB935502, 2010CB327704) and the National Natural Science Foundation of China (NSFC 50702057, 50872131, 20921002).

■ REFERENCES

(1) Dresselhaus, M. S.; Chen, G.; Tang, M. Y.; Yang, R. G.; Lee, H.; Wang, D. Z.; Ren, Z. F.; Fleurial, J. P.; Gogna, P. *Adv. Mater.* **2007**, *19*, 1043–1053.
(2) Wise, F. W. *Acc. Chem. Res.* **2000**, *33*, 773–780.
(3) Rogach, A. L.; Eychmüller, A.; Hickey, S. G.; Kershaw, S. V. *Small* **2007**, *3*, 536–557.
(4) Snyder, G. J.; Toberer, E. S. *Nat. Mater.* **2008**, *7*, 105–114.
(5) Lin, Y. M.; Dresselhaus, M. S. *Phys. Rev. B* **2003**, *68*, 075304.
(6) Harman, T. C.; Taylor, P. J.; Walsh, M. P.; LaForge, B. E. *Science* **2002**, *297*, 2229–2232.
(7) Urban, J. J.; Talapin, D. V.; Shevchenko, E. V.; Murray, C. B. *J. Am. Chem. Soc.* **2006**, *128*, 3248–3255.
(8) Cho, K.-S.; Talapin, D. V.; Gaschler, W.; Murray, C. B. *J. Am. Chem. Soc.* **2005**, *127*, 7140–7147.
(9) Talapin, D. V.; Murray, C. B. *Science* **2005**, *310*, 86–89.
(10) Murphy, J. E.; Beard, M. C.; Norman, A. G.; Ahrenkiel, S. P.; Johnson, J. C.; Yu, P. R.; Micic, O. I.; Ellingson, R. J.; Nozik, A. J. *J. Am. Chem. Soc.* **2006**, *128*, 3241–3247.
(11) Heremans, J. P.; Jovovic, V.; Toberer, E. S.; Saramat, A.; Kurosaki, K.; Charoenphakdee, A.; Yamanaka, S.; Snyder, G. J. *Science* **2008**, *321*, 554–557.
(12) Brumer, M.; Kigel, A.; Sashchiuk, A.; Bashouti, M.; Sirota, M.; Galun, E.; Burshtein, Z.; Le Quang, A. Q.; Ledoux-Rak, I.; Zyss, J. *J. Phys. Chem. B* **2006**, *110*, 25356–25365.
(13) Ma, W.; Luther, J. M.; Zheng, H.; Wu, Y.; Alivisatos, A. P. *Nano Lett.* **2009**, *9*, 1699–1703.
(14) Mokari, T.; Banin, U. *Chem. Mater.* **2003**, *15*, 3955–3960.
(15) Mokari, T.; Habas, S. E.; Zhang, M.; Yang, P. *Angew. Chem., Int. Ed.* **2008**, *47*, 5605–5608.
(16) Smith, D. K.; Luther, J. M.; Semonin, O. E.; Nozik, A. J.; Beard, M. C. *ACS Nano* **2011**, *5*, 183–190.
(17) Lu, W.; Fang, J.; Ding, Y.; Wang, Z. L. *J. Phys. Chem. B* **2005**, *109*, 19219–19222.
(18) Lu, W.; Fang, J.; Stokes, K. L.; Lin, J. *J. Am. Chem. Soc.* **2004**, *126*, 11798–11799.
(19) Lu, W.; Gao, P.; Jian, W. B.; Wang, Z. L.; Fang, J. *J. Am. Chem. Soc.* **2004**, *126*, 14816–14821.
(20) Zhang, J.; Kumbhar, A.; He, J.; Das, N. C.; Yang, K.; Wang, J.-Q.; Wang, H.; Stokes, K. L.; Fang, J. *J. Am. Chem. Soc.* **2008**, *130*, 15203–15209.
(21) Lu, W.; Ding, Y.; Chen, Y.; Wang, Z. L.; Fang, J. *J. Am. Chem. Soc.* **2005**, *127*, 10112–10116.
(22) Quan, Z. W.; Fang, J. Y. *Nano Today* **2010**, *5*, 390–411.
(23) PbSe and PbTe nanocubes were prepared using the same approach. They possess almost identical cubic morphology with the same size (~11 nm).
(24) Xu, D.; Bliznakov, S.; Liu, Z.; Fang, J.; Dimitrov, N. *Angew. Chem., Int. Ed.* **2010**, *122*, 1304–1307.
(25) Zhang, J.; Yang, H.; Yang, K.; Fang, J.; Zou, S.; Luo, Z.; Wang, H.; Bae, I.-T.; Jung, D. Y. *Adv. Funct. Mater.* **2010**, *20*, 3727–3733.
(26) Williams, D. B.; Carter, C. B. *Transmission Electron Microscopy: A Textbook for Materials Science; Spectrometry*, Part 4; Springer: New York, 2009; p 598.